RSC Advances

RSC Advances

ARTICLE

Revisited water radiolysis at elevated pH by accounting $O_3^{•−}$ kinetics at low and high LET

A. K. El Omar,[a] G. Baldacchino,*[b] I. Monnet[c] and P. Bouniol[a]

Ozonide radical, $O_3^{•−}$, is used in this study for probing radiolytic species formed in the radiolysis of liquid water at elevated pH. Its formation allows the scavenging of $O^{•−}$ whereas its disappearing is due to its reactions with $HO_2^−$ and $O_2^{•−}$. This article focuses on the formation and the reaction of $O_3^{•−}$ at pH 13.2 by using pulse radiolysis technique, with 10 M electrons and 1 GeV C^{6+} ions beams for the first time. This allowed us to work with two different Linear Energy Transfer (LET) values (0.27 and 33 eV/nm respectively), which means with two different primary distributions of radiolytic species. Consequently the rates constant of reactions $O_3^{•−}+HO_2^−$ and $O_3^{•−}+O_2^{•−}$ could be revised with acceptable accuracy thanks to deterministic simulations: $(1.1 \pm 0.2) \times 10^6$ $M^{-1}s^{-1}$ and $(1.5 \pm 0.5) \times 10^7$ $M^{-1}s^{-1}$ respectively. Furthermore, the primary radiolytic yields of $HO^•/O^{•−}$ and $H_2O_2/HO_2^−$ at high LET and pH 13.2 were estimated at 6.5 and 9.6×10^{-8} $mol.J^{-1}$ respectively which corresponds to the literature values.

Introduction

Radiation chemistry of water has been widely investigated in the last 50 years with a large literature concerning water at neutral pH as it can be exploited in recent reviews, reports or books.[1-4] More recently attention was paid on extreme conditions in radiation chemistry of water and particularly on the temperature range extended to supercritical conditions of water especially for converging to the next generation of nuclear reactor or the understanding of phenomena under conditions of nuclear accidents .[5] Going to more and more mimicking the real conditions in the industry, researches were focused on mixing the conditions lying on temperature elevation and high Linear Energy Transfer (LET = -dE/dx) irradiations.[6] Evidently the complexity of acquiring the data in term of radiolytic yields or rate constants was becoming higher and only few articles are available. That is the similar explanation of why no coupling exists between high LET irradiation and extreme pH variations. Extreme pH exists in real conditions, in nuclear industry. It is a particular case of extremely high concentrated solutions under radiation that causes problems of interpretation of complex reaction mechanisms (see for example ref.7).[7] Extremely low pH is used to dissolve nuclear spent fuel whereas high alkaline pH has to be considered in the pore solution of cement-based materials used in the nuclear wastes conditioning.[8] The presence of a residual aqueous solution within the material pores is considered to be the cause of enhanced H_2 production since the liquid is in interaction with the ionizing radiation, inducing its decomposition.[8] Actually the interstitial solution is known for its high pH value (> 13). In the history of radiation chemistry this latter conditions (ie high pH) were investigated by Hayon,[9] and Haissinsky[10] in the 60's under γ-rays provided by a ^{60}Co source. In 2000, Ferradini and Jay-Gerin claimed that effect of pH is still an open question especially for the determination of radiolytic yields.[11] Tentative Monte Carlo simulations in 2005 by Cobut et al. showed that molecular hydrogen yields were not sensitive to pH in the range 1 to 13.[12] Since evaluating the radiolysis effects on cement matrices in a century is still on demand especially in terms of hydrogen release, methods must be proposed to obtain better accuracy of input data which are necessary to simulate chemical processes in pore solution at long term. The evolution of radiolytic yields at high pH or high LET (under alpha irradiation for instance) is known separately and conceptually which means without enough accuracy.[13] The reactions involved in the chemical processes in non-homogeneous and in homogeneous stages of the radiolysis scheme are not known at all due to the equilibria involved for the formed radical species themselves when pH becomes extreme. In these conditions, the rate constants must be determined with the highest precision even for the slowest supposed reactions. As it is shown in Table 1, many reactions involving Reactive Oxygen Species (ROS)[14] in alkaline context are of this type and among them the controversial Haber-Weiss reaction[15] (presented in Reaction A in neutral solution) is for example a case that should be revisited.

$$HO_2^• + H_2O_2 \rightarrow HO^• + H_2O + O_2 \qquad (48)$$
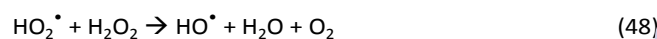
a. CEA Saclay, DEN, DPC, SECR, Laboratoire d'étude du comportement des bétons et des argiles, F-91991, Gif-sur-Yvette, France.
b. CEA Saclay, DSM, IRAMIS, LIDyL-LFP, URA 2453, F-91991, Gif-sur-Yvette, France. E-mail : gerard.baldacchino@cea.fr
c. CIMAP-ENSICAEN-CEA-CNRS-University of Caen, Bd H. Becquerel, BP 5133, 14070, Caen Cedex 5, France.
DOI: 10.1039/x0xx00000x

Several research groups tried to study the Haber-Weiss reaction qualitatively and they concluded that the reaction either does not occur,[16] either is very slow.[17, 18] It is the case for the basic form for which the rate constant is estimated to 8.23×10^{-2} $M^{-1}s^{-1}$.[19] Also reported by direct observation in the gas phase,[20] the Haber-Weiss reaction in solution is a secondary source for O_2 and $O^{\bullet-}$ which can react and produce easily ozonide radical, $O_3^{\bullet-}$ as followed, presented in alkaline solution within a long chemical mechanism (Table 1):

$$O_2^{\bullet-} + HO_2^- \rightarrow O^{\bullet-} + O_2 + HO^- \quad (41)$$
$$O^{\bullet-} + O_2 \rightarrow O_3^{\bullet-} \ (k = 3.7 \times 10^8 \ M^{-1} \ s^{-1})^8 \quad (28)$$
$$O_3^{\bullet-} \rightarrow O^{\bullet-} + O_2 \ (k = 2.6 \times 10^3 \ M^{-1} \ s^{-1})^8 \quad (51)$$

Monitoring ROS should allow us to elaborate a complete reaction scheme in alkaline media since they are involved in secondary reactions which enter in competition with the Haber-Weiss once. As recently published by Si *et al.* the $O^{\bullet-}$ formation can be analyzed by using a specific fluorescent dye as scavenger during hydrogen peroxide decomposition under a temperature elevation in alkaline solution and without irradiation effect[21]. But $O^{\bullet-}$ is involved in many reactions in water radiolysis and its scavenging would be difficult to interpret. In oxygen saturated solution, $O_3^{\bullet-}$ should be then potentially a more recommended species for the detection of $O^{\bullet-}$ scavenged by molecular oxygen (Reaction 28). Above all, $O_3^{\bullet-}$ absorbs in the visible region with a maximum located at 430 nm (see the spectra in Figure 1).[22]
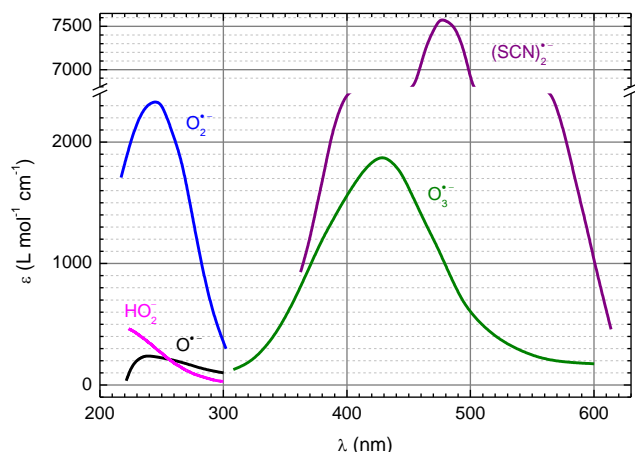
Fig. 1 UV-visible spectra of species present in aerated alkaline solution ($O^{\bullet-}$, HO_2^-, $O_2^{\bullet-}$ and $O_3^{\bullet-}$) under radiation or used in the chemical dosimetry (($SCN)_2^{\bullet-}$). These spectra come from literature.[22-24]

Moreover, on the one hand, considering a pH value of 13.2 and the $pKa(HO^{\bullet}/O^{\bullet-})$ value of 11.6, a majority of $HO^{\bullet}$ is converted into $O^{\bullet-}$ directly in the tracks (*vide infra*, Reaction 64 in Table 2), and on the other hand, a typical concentration O_2 of 10^{-3} M in oxygen saturated solution should scavenge $O^{\bullet-}$ within the microsecond time scale regarding Reaction 28 in the whole radiolysis scheme[13]. That means $O^{\bullet-}$ should be scavenged as a primary species. We can have a similar

discussion with H_2O_2/HO_2^- which is particularly involved in Reaction 41 and for which pKa value is 11.75.

The idea of the present study is to use the detection of $O_3^{\bullet-}$ for determining both rate constants involving this freshly formed species and the primary yield of $HO^{\bullet}/O^{\bullet-}$ at pH 13.2 at two LET values provided by 10 MeV electrons and 1 GeV Carbon ions. As far as we know this is the first time those conditions are encountered and studied in the literature. Those are close to the conditions encountered in the cement used for the waste conditioning in nuclear industry.

In the following study, the effect of two parameters will be monitored through the absorption kinetics of $O_3^{\bullet-}$: the presence of various concentrations of hydrogen peroxide and the ionizing particles having two different LET values. The initial distributions being very different in terms of G-values and/or initial concentrations of H_2O_2 will favor some reactions in the competitive mechanism, especially in the long-term reactions (i.e. 100 µs – 1 s range). This method using various LET values as a competition parameter has been already used successfully in the past.[25] Then the comparison of the kinetics will allow the simulation of the experimental data by revisiting these reactions, and when it is necessary, their rate constants in the mechanism of alkaline water radiolysis. Furthermore, the determination of primary radiolytic yield of $HO^{\bullet}/O^{\bullet-}$ and H_2O_2/HO_2^- at high LET will be attempted.

Materials and methods

All alkaline solutions were prepared by dissolving NaOH pellets into pure water. The investigated NaOH concentration was equal to 0.24 M which insured a pH of 13.2 in the medium. H_2O_2 was added into the medium prior to irradiations and four concentrations were investigated: 0, 0.1, 0.2 and 0.5 mM. NaOH pellets were purchased from Sigma-Aldrich and were of the highest purity (> 99%). H_2O_2 solution was purchased from Acros Organics (30 wt% in water) and was non-stabilized. All chemical reagents were used without any further treatment. Ultra-pure water (18.2 MΩ·cm) from Milli-Q Millipore System has been used in the preparation of solutions. All solutions were prepared in a glove box under inert atmosphere (Ar gas of the highest purity) in order to properly weight NaOH pellets at a minimum humidity rate (≤ 6.5 %).

After their preparation, and prior to their irradiation, solutions were bubbled with oxygen during an hour to insure the saturation of the medium with $O_{2(g)}$. During irradiations, solution tanks were also continuously kept under O_2 bubbling. The pulse radiolysis setups used for both types of accelerated particles, electrons and C^{6+} ions, have been described elsewhere.[26-29] Briefly, in both cases, the same irradiation flow cell has been used. The cell is purchased from Hellma Analytics, and is made of Suprasil® silica. Both width and depth are equal to 12.5 mm, and knowing that the width of silica is equal to 3 mm per side, the ionizing radiation passes through 6.5 mm of solution. The cell holds 750 µL of solution and is renewed after each acquisition. Optical path is equal to 1 cm and the light source used in our study is a 405 nm laser diode purchased from Oxxius. The transmitted light is then detected with a Silicon photodiode and through adjustable impedance

(Thorlabs). Signal is then digitalized by a fast oscilloscope (Tektronix, DPO 7254).

Pulse radiolysis experiments

Electron pulse radiolysis experiments were performed using a 10-MeV electron accelerator (ALIENOR) providing electron pulses with duration of 10 ns and repetition rate of 0.5 Hz.[29] Two acquisition time-ranges were recorded, long (50 ms) and short (200 μs). The delivered dose was determined using potassium thiocyanate solution (KSCN, 10^{-2} M) saturated with $N_2O_{(g)}$ as a dosimetry system.[30,31] The determination of $(SCN)_2^{\bullet-}$ concentration (Figure 1) leads to a dose value of 84 ± 5 Gy/pulse.

Pulse radiolysis with $^{13}C^{6+}$ of 1.23 GeV (95 MeV/nucleon) was performed at GANIL cyclotron facility. Pulse duration was 100 μs with a repetition period of 500 ms.

Energy deposition in the medium, corresponding to the Linear Energy Transfer (LET) defined as LET = $-(dE/dX)_{elec}$,[13] along the trajectory of the solution/irradiation interaction was calculated using SRIM software[32], and is shown in Figure 2. An average value of 33 eV·nm^{-1} is found for LET. Note that 10 MeV electrons have an LET of 0.27 eV·nm^{-1}.[13] A dose of 12.5 Gy/100-μs-pulse was then determined using the LET value and the ion flux (3×10^8 ions/s)).

Deterministic simulation of the radiolysis

Simulation of the chemical mechanism of radiolysis of alkaline water has been carried out with an ad hoc differential equations system solver, Chemsimul.[33] It represents a computerized chemical simulator which is used, in our case, for translating the input series of chemical reactions, following the irradiation of alkaline water, into differential equations. Therefore, this code is used for simulating the homogeneous chemistry considering the primary yields (G-values) distribution of species escaped from recombination in the non-homogeneous stage of the radiolysis scheme.[34] Then, the obtained result represents a prediction of the behaviour of radical and molecular species over a defined period of time. For this purpose, several parameters need to be defined in the code before performing the simulations. Among those parameters we mention the rate constant of chemical reactions, G-values of radical and molecular species (a collection is presented in Table 3 for electron beam and C^{6+} beam), initial concentrations of solutes, medium temperature (T (K)), irradiation mode (single shot or pulse train), time duration of the irradiation, irradiation dose and simulation time. Details regarding the constituents of Chemsimul codes can be found elsewhere.[19, 33]

Simulations for both irradiation systems followed after collecting the experimental data. For this purpose an input file containing the same reactional mechanism of water radiolysis was used (Tables 1 and 2). Both input files were identical except for some differences related to the delivered dose, pulse duration, and for the G-values of radicals and molecules (Table 3).
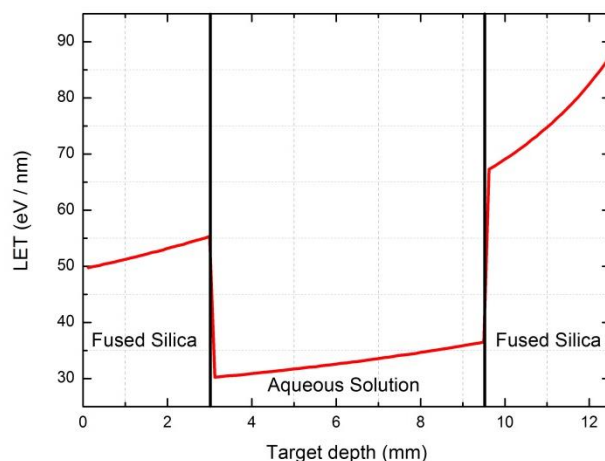
Fig. 2 Energy deposition of $^{13}C^{6+}$ ions of incident energy of 1.13 GeV, in alkaline medium, calculated using SRIM software. Within the aqueous medium, LET variation can be considered as negligible and the average value is 33 eV·nm^{-1}.

Initial composition of the alkaline solution, i.e. initial concentration species prior to irradiation, was determined using Mathematica® software. For this purpose, the knowledge of parameters such as the ionic product of water,[35] and water density at a precise temperature,[36] 24.5 °C for this work, is required in order to compute ionic strength and activity coefficients (Debye-Hückel model with Davies extension).

Results

In this study, obtained results focus on the reactivity of $O_3^{\bullet-}$ radical anion following the irradiation of water alkaline solutions in presence of various concentrations hydrogen peroxide. Our choice of studying this ROS ($O_3^{\bullet-}$) was made even easier due to its relatively long half-life, its exclusive presence in alkaline condition due to its $pKa(HO_3^{\bullet}/O_3^{\bullet-}) = 6.45$,[37] and knowing that its absorption spectrum exhibits its maximum at 430 nm (ε_{430nm} = 1900 M^{-1}·cm^{-1}).[22, 38] Thus, transient absorption of $O_3^{\bullet-}$ radical anion can be monitored without the need of any further treatment of the spectrum interferences of other ROS.

Irradiations were performed using two types of accelerated particles, 10 MeV-electrons and 1 GeV-C^{6+} corresponding to low (0.27 eV·nm^{-1}) and high (33 eV·nm^{-1}) LET values, respectively. As a consequence of LET variation, the G-values distribution of radicals (e_s^-, $HO^{\bullet}/O^{\bullet-}$ and $H^{\bullet}$) and molecular species (H_2O_2/HO_2^- and H_2) change. One can see the distributions in Table 3. As a consequence of the LET variation, the chemistry taking place in the irradiated medium can vary, due to the present quantities of species which are readily available for interaction.

Electron Irradiation

10 MeV-electrons were used to irradiate NaOH solutions in presence of 4 concentrations of H_2O_2 going from 0 to 5×10^{-4} M. Figure 3 represents transient absorption recorded at 405 nm,

where upper and lower graphs correspond to long (30 ms) and short (165 µs) acquisitions time scales, respectively. In the case of the lower graph, transient absorption of black, red and blue plots, corresponding to the addition of 0, 10^{-4} and 2 x 10^{-4} M H_2O_2 respectively were arbitrary separated by using a convenient factor.

Thus, the influence of presence of various concentrations of H_2O_2 can be shown clearly. The upper graph shows the real absorbance values. In the lower graph, following the passage of the ionizing radiation (at t=0), the $O_3^{\bullet-}$ rise, during a few µs, is attributed to the time-resolution limitation due to the 5 kΩ impedance plugged to the oscilloscope. As a result this rise is not easily analyzed. Then this is followed by a decay of the transient absorption signal. It is attributed to the reactivity of $O_3^{\bullet-}$ over the time window of acquisition. Aside from this latter species, hydrated electron could also contribute to the observed absorption due to its broad absorption spectrum extending over UV-Vis and NIR ranges.[22] But, since the solution is saturated with $O_{2(g)}$ (1.3 x 10^{-3} M),[39] and since it represents an excellent scavenger for solvated electron (Reaction 9, Table 1), contribution of the solvated electron to the observed transient absorption is shortened and negligible.

For both graphs in Figure 3, we can notice that $O_3^{\bullet-}$ decay becomes faster when the amount of added H_2O_2, prior to irradiation, increases. This is mainly attributed to the reaction of $O_3^{\bullet-}$ with HO_2^- (Reaction 52 in Table 1). In fact, due to medium's pH, H_2O_2 will react with HO^- in order to form the hydroperoxide anion (HO_2^-) (Table 2). Thus, the presence of HO_2^- with such important quantities makes it readily available for reaction with ozonide radical anion, which can explain the observed faster decays as a function of the initially added hydrogen peroxide solution.

C^{6+} ions irradiation

$^{13}C^{6+}$ (1.23GeV) ions have been used to irradiate oxygen saturated aqueous sodium hydroxide solutions, of a concentration of 0.24 mol·dm^{-3} corresponding to a pH of 13.2, in presence of several concentrations of H_2O_2 going from 0 to 5×10^{-4} mol·dm^{-3} similarly to the 10 MeV-electrons irradiations. Absorption kinetics were obtained using the pulse radiolysis technique where C^{6+} pulse trains, with a pulse duration of 100 µs and repetition period of 500 ms (except for no-added H_2O_2 kinetics where single shot was used), were delivered by GANIL cyclotron.

Figure 4 presents recorded kinetics at 405 nm following the irradiation of sodium hydroxide aqueous solutions with carbon ions. Black, red, green and blue dotted plots represent experimental kinetics corresponding to 0, 10^{-4}, 2×10^{-4} and 5×10^{-4} M of added H_2O_2, respectively. The passage of C^{6+} through the different media led, like in the case of electron beams, to the formation and then decay of $O_3^{\bullet-}$ over the temporal acquisition window (17 ms). It is important to note that again hydrated electron cannot contribute to the absorption at 405 nm for the similar reason than electron beam irradiation. We can add that due to irradiation with high LET beam primary yield of hydrated electron is much less than at low LET.[27]

From the absorbance amplitude point of view, one can notice that absorbance values are low (about 1.3×10^{-3} at maximum) and lower of about a factor of 10 than under electron beam irradiations. This

is mainly due to the lower dose per pulse (12.5 Gy whereas 84 Gy for electron pulses) and a probable lower $O^{\bullet-}$ G-value than at low LET irradiation (similarly than in neutral pH conditions for $HO^{\bullet}$ G-value[6, 40]). Formation of $O_3^{\bullet-}$ radical anion is complete within the 100 µs of the C^{6+} pulse.
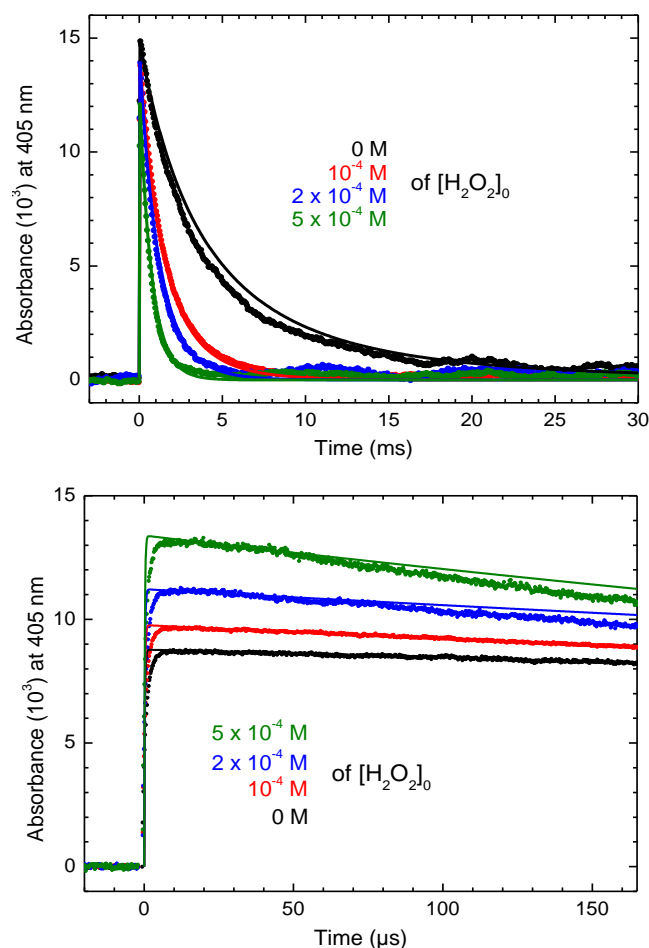
Fig. 3 Transient absorbance recorded at 405 nm following the irradiation of oxygen saturated NaOH aqueous solutions (0.24 mol·dm^{-3}) with 10 MeV-electron pulse (10 ns, 0.5 Hz). Dose per 10 ns-pulse was around 84 Gy. Upper and lower graphics correspond to long (50 ms) and short (165 µs) acquisition time scales. Alkaline solution contained four H_2O_2 initial concentrations: 0, 10^{-4}, 2×10^{-4} and 5×10^{-4} mol·dm^{-3} corresponding to black, red, green and blue dotted plots, respectively. Solid lines observed in the lower graph represent simulations. In order to make the figure easier to read, black, red and blue plots of the lower graph have been each divided by a convenient factor: 1.5, 1.3 and 1.2, respectively.

Considering the decay stage, one can also note that without added H_2O_2, $O_3^{\bullet-}$ decays faster than under low LET irradiation. Nevertheless under high LET irradiation H_2O_2 G-value is greater than under low LET: from a value of 7×10^{-8} under γ-rays to 9-10×10^{-8} mol/J[41]. This change of primary yield affects the initial condition like an added concentration of H_2O_2. This addition would correspond to a concentration of 2.5×10^{-7} M which cannot explain itself this acceleration. To understand this phenomenon we must look at the concentrations of $O_3^{\bullet-}$ and

$O_2^{\bullet-}$ formed in the pulse. Both of them are high at low LET because they follow the scavenging reactions of $O^{\bullet-}$ and of hydrated electron. These two primary species have greater G-values under low LET irradiation than under high LET one. With a LET of 0.27 eV/nm, these G-values are about 2.7×10^{-7} mol/J which correspond to "initial" concentrations of $O_3^{\bullet-}$ and $O_2^{\bullet-}$ of 2.3×10^{-5} M respectively. The $O_3^{\bullet-}$ and $O_2^{\bullet-}$ implication in the radiolysis process is complex by following both second order laws (disproportionation Reaction 43) and combined reactions like Reaction 45. Then their concentrations can rapidly decline. Therefore it is probably the main reason why $O_3^{\bullet-}$ decay is faster at low LET value.
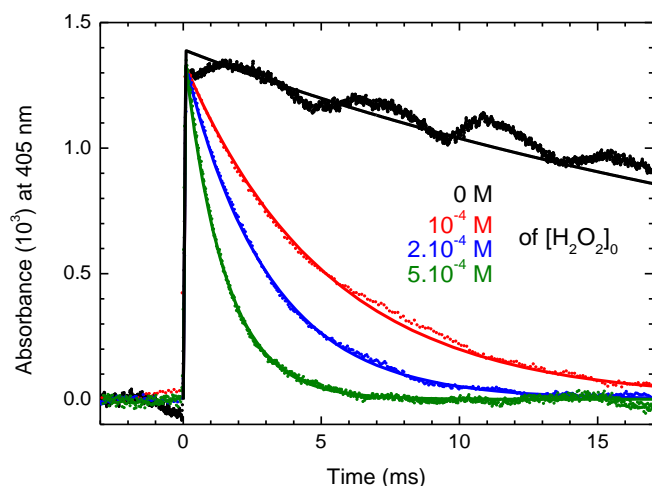
Fig. 4 Transient absorbance recorded at 405 nm following the irradiation of NaOH aqueous solutions (0.24 mol·dm^{-3}) with C^{6+} 95 MeV/A. Solution contained various concentrations of H_2O_2 injected into the medium prior to irradiations, and H_2O_2 initial concentrations were equal to 0, 10^{-4}, 2×10^{-4} and 5×10^{-4} mol·dm^{-3} corresponding to black, red, green and blue dotted plots, respectively. Solid line plots are simulations. Dose per 100 µs-pulse was 12.5 Gy. Due to the long lived ozonide without added H_2O_2, the kinetics was recorded with single shot mode. All Solutions were saturated with molecular oxygen prior to irradiation.

More over when the concentration of added H_2O_2 increases decay is again faster. In fact, following the addition of H_2O_2, and due to the high pH value of the medium, H_2O_2 is immediately converted into its alkaline equivalent, HO_2^-, through the acid base equilibrium consisting of both Reactions 73 and 74 (Table 2). $O_3^{\bullet-}$ and HO_2^- can react following Reaction 52. Moreover the rate of the decays seems faster for high-LET records than the ones at low LET. This important LET effect is logically attributed to a significant difference in the radiolytic yield distribution between high and low LET experiments.

Simulations and adjustment of k_{45}, k_{52} and $G(H_2O_2)$
After obtaining the data from the radiolysis of aqueous NaOH solutions using energetic electrons and C^{6+} ions, we proceeded by performing simulations using a set of reactions as a model for the mechanism of water radiolysis in alkaline conditions. The obtained results showed significant deviations from the experimental kinetics implying that one or several rate constant values of reactions used in the model and shown in Table 1 need to be re-evaluated. Table 1 collects 60 reactions

which constitute the mechanism of water radiolysis used in this study. The background colors are used to differentiate reactions revisited by Elliot and Bartels in 2009,[2] written over green background and representing half of Table 1, from the ones not mentioned in their report. Our choice in separating reactions into two groups was being supported by our need to reduce the number of parameters, in this case rate constant values, which might require adjustment in order to properly fit the experimental recorded kinetics. Following this reasoning, we considered that all reactions mentioned in Elliot and Bartels report do not require further investigation and that the rest might require some revisiting procedure following the fact that the new technological advances and this new current approach allow us to determine rate constant of reactions more precisely than it had been done in the past.

Add to that rate constants of simple reaction cannot be adjusted in a complex reaction mechanism without accounting the effect of the whole mechanism. We have noticed previously that $O_3^{\bullet-}$ is involved in several reactions and makes its kinetics impossible to fit with a simple order reaction law. Also previously noticed is the consequences of LET value that affects the observable rates. The previous section has finally concluded that an adjustment of the rate constant k_{52} should be better in high LET condition instead of k_{45} under low LET one. Therefore we proceeded an iteration between simulations at high and low LET of the respective experimental kinetics, adjusting first k_{52} to $O_3^{\bullet-}$ kinetics in the former condition, then k_{45} to $O_3^{\bullet-}$ kinetics in the latter condition.

The results of these iterations are the found values of k_{52} and k_{45}: $1.1\pm0.2 \times 10^6$ and $1.5\pm0.5 \times 10^7$ M$^{-1}\cdot$s^{-1} respectively. Figures 2 and 3 include simulations obtained using Chemsimul software including the whole mechanism depicted in Tables 1 and 2 and the novel values of k_{52} and k_{45}. Actually the best agreement with experimental results was obtained when the rate constant k_{52} is fixed at 1.1×10^6 instead of 8.9×10^5 M$^{-1}\cdot$s^{-1} found in literature.[42] At this stage, note also that k_{45} value was fixed arbitrarily to 10^4 M$^{-1}\cdot$s^{-1} in the literature up to now.[38]
Following the determination of these rate values, we then proceeded by performing the same simulation for NaOH solutions, saturated with O_2, without addition of H_2O_2, and irradiated using C^{6+} swift ions. Actually, the presence of added H_2O_2 has shown the influence of H_2O_2 but it has masked the intrinsic H_2O_2 formed as a primary product of water radiolysis and made its influence negligible. As a consequence, in absence of added H_2O_2, simulations should be sensitive towards the modification of $G(H_2O_2/HO_2^-)$ value. The effect is presented in Figure 5. Along with the reference values (Table 3, first line for C^{6+} ions) taken for this work and corresponding to the green solid line, three other values were used for the simulations: 0.5, 1.5 and 2 molecules/100 eV. Comparing to the experimental results, all simulated plots seem to be in good agreement with our scattered data. Moreover we are aware that a fitting of full range kinetics would have brought a better precision to the G-value adjustment but it was impossible due to the slow decay and the perturbation visible in Figure 4. Therefore experimental transient absorption within an accuracy of 10^{-4} in absorbance suggests that signal of

$O_3^{\bullet-}$ alone is not sufficient in the precise determination of $G(H_2O_2)$. It is important to note that the G-values for C^{6+} ions irradiation were then used in the input files of all the studied systems.
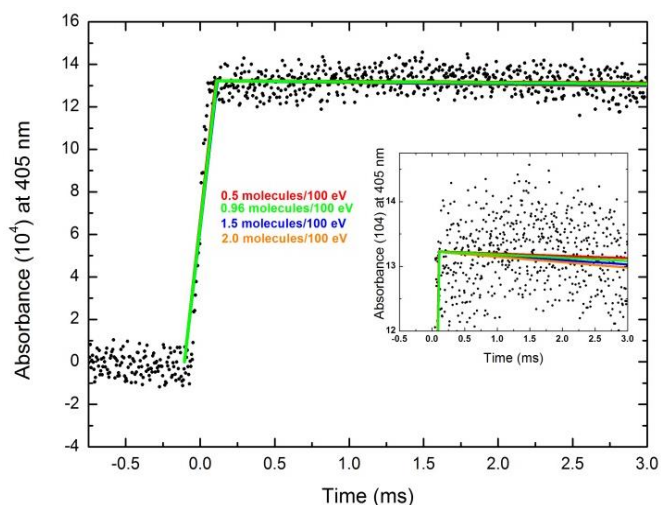
Fig. 5 Transient absorbance recorded at 405 nm following the irradiation of O_2 saturated NaOH aqueous solutions (0.24 mol·dm^{-3}) with C^{6+} of 95 MeV/A. Solid lines represent simulations where red, green, blue, and orange lines correspond to 0.5, 0.96, 1.5, and 2.0 molecules/100 eV for $G(H_2O_2)$, respectively. The inset plot represents a zoom of the transient absorption at 405 nm following the passage of C^{6+} ions beam.

Discussion

The particularity of the system we are studying is that its radiolysis leads to the formation of several ROS. $O^{\bullet-}$ and $O_2^{\bullet-}$ are both known to have their respective absorption spectrum in the same UV range,[43-45] making their detection and separation a complicated task. Thus, $O_3^{\bullet-}$ represented an interesting species for our studies since: 1- it has a major role in the mechanism of water radiolysis in alkaline and aerated conditions, 2- some of its reactions are satellite reactions of the Haber-Weiss one (Reactions 41 and 42, Table 1), and 3- its absorption spectrum lies in the visible region without being overlapped by the absorption of any other ROS.[38]

Then $O_3^{\bullet-}$ has been studied by irradiating aqueous solutions of NaOH of a concentration of 0.24 M, the equivalent of pH 13.2 that matches the pH found in cement based materials used for radwaste conditioning.[8] Energetic electrons and C^{6+} ions were used as pulsed radiation sources. The use of heavy ions having high LET was motivated by the need to minimize the quantities of formed radical species in the medium. It artificially allows the changes in the initial distribution of concentration of each radiolytic species: G-values distribution can disturb the following chemistry and makes some reactions favored in the big competition including more than 50 reactions. In fact, knowing the important number of reactions which might potentially require adjustments, we used heavy ions as irradiation source in order to limit the quantities of transient ROS species present in the medium, thus minimizing their influence through their reactivity through secondary and satellite reactions. This approach allowed us to concentrate on the reactivity of $O_3^{\bullet-}$ without having to worry about oxide and

superoxide reactivity. This method is used for the first time to determine rate constants in alkaline solutions.

The formation and decay kinetics of $O_3^{\bullet-}$ presented in Figure 4 were then simulated using the Chemsimul code and we found that even a slight variation of Reaction 52 will have a direct impact on the simulated behavior of the transient absorption. The performed simulations led us to properly fit the experimental kinetics by considering k_{52} to be equal to $(1.1 \pm 0.2) \times 10^6$ M^{-1}·s^{-1}. This value is slightly higher than $(8.9 \pm 1.1) \times 10^5$ M^{-1}·s^{-1} and slightly lower than 1.6×10^6 M^{-1}·s^{-1} reported by Felix et al.,[42] and Czapski in 1967,[46] respectively. The slight differences between the reported values can be attributed to the long kinetic acquisitions, since the main difficulties in such acquisitions lie in the stability of the light source used for the study, the presence of impurities and the photodecomposition of hydrogen peroxide due to the analyzing light source. In fact, for long time scales, light sources exhibit some intensity fluctuations which can affect the recorded kinetic. Add to that, a potential impurity can react with any of the present species in the irradiated medium (radical and/or molecular species) causing a change in the chemistry taking place in the medium and thus affecting the evaluation of rate constant values of reactions of interest. For this reason, special care has been brought to the used water, glassware and used chemicals.[47] Moreover, when intense light sources are used, it is well known that the interaction between light and HO_2^- can lead to the photodecomposition of this latter species as shown in the Reactions 79 and 80.[48]

$$HO_2^- + h\nu \rightarrow HO^{\bullet} + O^{\bullet-} \qquad (79)$$
$$HO_2^- + h\nu \rightarrow HO^- + O(^3P) \qquad (80)$$

Accompanying the change of k_{52}, it was necessary to adjust the rate constant of Reaction 45 at $1.5 \pm 0.5 \times 10^7$ M^{-1}·s^{-1}. k_{45} was fixed up to now to 10^4 M^{-1}·s^{-1} by Sehested et al. who have never considered the occurrence of Reaction 52 in their experiments/simulations under high pressure of oxygen.[38] In these conditions they observed very long lifetime of $O_3^{\bullet-}$ decaying with a no-order reaction. This imposed that Reaction 45 might not play an important role in the mechanism. We now suggest it plays a relatively more important role (multiplied by a factor of 1.5×10^3) provided that it is compensated by the consideration of Reaction 52.

Furthermore, it was also noted that any change in the radiolytic yield value of H_2O_2/HO_2^-, $(G(H_2O_2/HO_2^-))$, does not have any significant effect on the simulated kinetics, when H_2O_2/HO_2^- was initially present in solutions prior to their irradiations, making the quantities of H_2O_2/HO_2^- formed during the irradiation process negligible and with a negligible effect. Add to that, the difference in reactivity between the solution with no H_2O_2 and the three others containing initial quantities of H_2O_2 strongly suggests that the mechanism of alkaline water radiolysis is not optimized highlighting, again, the need for revisiting rate constant values of some of the ROS reactions. Then, following the determination of k_{52} using the irradiation of NaOH solution with C^{6+} ions and in presence of H_2O_2 and the

Journal Name

ARTICLE

validation of the value when electrons were used as source of ionizing radiation, we performed the same simulation for NaOH aqueous solution, irradiated with C^{6+}, in absence of H_2O_2 prior to the irradiation in an attempt to determine $G(H_2O_2/HO_2^-)$, under high LET ionizing radiation. The results shown in Figure 5 clearly indicate that even any change in

$G(H_2O_2/HO_2^-)$ does not seem to have a considerable impact on the simulated kinetic behavior.

Table 1 List of reactions involved in the mechanism of water radiolysis in presence of oxygen. Reactions written on green background were revised by Elliot and Bartels in 2009,[2] and are considered in our calculations without any further consideration. Reaction 45 and 52, with an orange background, are mentioned with their original rate constant and are revisited in this present study.

Number	Reaction	k (s^{-1} or M^{-1} s^{-1})	Ref.
1	$e_{aq}^- + e_{aq}^- \rightarrow H_2 + 2HO^-$	7.3×10^9	2
2	$e_{aq}^- + H^\bullet \rightarrow H_2 + HO^-$	2.8×10^{10}	2
3	$e_{aq}^- + O^{\bullet-} \rightarrow 2HO^-$	2.3×10^{10}	49
4	$e_{aq}^- + HO^\bullet \rightarrow H_2O + HO^-$	3.5×10^{10}	2
5	$e_{aq}^- + HO_2^- \rightarrow H_2O + O^{\bullet-} + HO^-$	3.5×10^9	49
6	$e_{aq}^- + H_2O_2 \rightarrow H_2O + HO^\bullet + HO^-$	1.4×10^{10}	2
7	$e_{aq}^- + O_2^{\bullet-} \rightarrow H_2O + O_2^{2-}$	1.3×10^{10}	2
8	$e_{aq}^- + HO_2^\bullet \rightarrow H_2O + HO_2^-$	1.3×10^{10}	2
9	$e_{aq}^- + O_2 \rightarrow H_2O + O_2^{\bullet-}$	2.3×10^{10}	2
10	$e_{aq}^- + O_3^{\bullet-} \rightarrow 2HO^- + O_2$	1.6×10^{10}	50
11	$e_{aq}^- + O_3 \rightarrow H_2O + O_3^{\bullet-}$	3.6×10^{10}	51
12	$H^\bullet + H^\bullet \rightarrow H_2$	5.1×10^9	2
13	$H^\bullet + H_2O \rightarrow H_2 + HO^\bullet$	3.0×10^{-3}	2
14	$H^\bullet + O^{\bullet-} \rightarrow HO^-$	2.0×10^{10}	52
15	$H^\bullet + HO^\bullet \rightarrow H_2O$	1.1×10^{10}	
16	$H^\bullet + HO_2^- \rightarrow HO^\bullet + HO^-$	1.4×10^9	53
17	$H^\bullet + H_2O_2 \rightarrow HO^\bullet + H2O$	3.6×10^7	53
18	$H^\bullet + O_2^{\bullet-} \rightarrow HO_2^-$	1.1×10^{10}	2
19	$H^\bullet + HO_2^\bullet \rightarrow H_2O_2$	1.1×10^{10}	2
20	$H^\bullet + O_2 \rightarrow HO_2^\bullet$	1.3×10^{10}	2
21	$H^\bullet + O_3 \rightarrow HO^\bullet + O_2$	2.2×10^{10}	51
22	$O^{\bullet-} + H_2 \rightarrow HO^- + H^\bullet$	1.3×10^8	2
23	$O^{\bullet-} + O^{\bullet-} \rightarrow O_2^{2-}$	1.0×10^8	54
24	$O^{\bullet-} + HO^\bullet \rightarrow HO_2^-$	7.6×10^9	49
25	$O^{\bullet-} + HO_2^- \rightarrow HO^- + O_2^{\bullet-}$	7.9×10^8	2
26	$O^{\bullet-} + H_2O_2 \rightarrow O_2^{\bullet-} + H_2O$	1.6×10^8	2
27	$O^{\bullet-} + O_2^{\bullet-} \rightarrow O^{2-} + O_2$	6.0×10^8	38
28	$O^{\bullet-} + O_2 \rightarrow O_3^{\bullet-}$	3.7×10^8	2
29	$O^{\bullet-} + O_3^{\bullet-} \rightarrow 2O_2^{\bullet-}$	7.0×10^8	38
30	$O^{\bullet-} + O_3 \rightarrow O_2^{\bullet-} + O_2$	1.0×10^9	55
31	$HO^\bullet + H_2 \rightarrow H_2O + H^\bullet$	3.9×10^7	2
32	$HO^\bullet + HO^\bullet \rightarrow H_2O_2$	4.8×10^9	2
33	$HO^\bullet + HO_2^- \rightarrow H_2O + O_2^{\bullet-}$	5.6×10^9	2
34	$HO^\bullet + H_2O_2 \rightarrow H_2O + HO_2^\bullet$	2.9×10^7	2
35	$HO^\bullet + O_2^{\bullet-} \rightarrow HO^- + O_2$	1.1×10^{10}	2
36	$HO^\bullet + HO_2^\bullet \rightarrow H_2O + O_2$	8.8×10^9	2
37	$HO^\bullet + O_3^{\bullet-} \rightarrow HO^- + O_3$	2.5×10^9	56
38	$HO^\bullet + O_3^{\bullet-} \rightarrow HO_2^\bullet + O_2^{\bullet-}$	6.0×10^9	56
39	$HO^\bullet + HO_3^\bullet \rightarrow O_2 + H_2O_2$	5.0×10^9	57
40	$HO^\bullet + O_3 \rightarrow HO_2^\bullet + O_2$	1.0×10^8	56
41	$O_2^{\bullet-} + HO_2^- \rightarrow O_2 + HO^- + O^{\bullet-}$	8.2×10^{-2}	19
42	$O_2^{\bullet-} + H_2O_2 \rightarrow O_2 + HO^- + HO^\bullet$	1.3×10^{-1}	47
43	$O_2^{\bullet-} + O_2^{\bullet-} \rightarrow O_2 + O_2^{2-}$	3.0×10^{-1}	45
44	$O_2^{\bullet-} + HO_2^\bullet \rightarrow O_2 + HO_2^-$	1.0×10^8	2
45	$O_2^{\bullet-} + O_3^{\bullet-} \rightarrow 2O_2 + O^{2-}$	1.0×10^4	50
46	$O_2^{\bullet-} + HO_3^\bullet \rightarrow 2O_2 + HO^-$	1.0×10^{10}	57
47	$O_2^{\bullet-} + O_3 \rightarrow O_2 + O_3^{\bullet-}$	1.5×10^9	51
48	$HO_2^\bullet + H_2O_2 \rightarrow O_2 + HO^\bullet + H_2O$	5.0×10^{-1}	47
49	$HO_2^\bullet + HO_2^\bullet \rightarrow O_2 + H_2O_2$	8.4×10^5	2
50	$HO_2^\bullet + O_3 \rightarrow HO^\bullet + 2O_2$	5.0×10^8	50
51	$O_3^{\bullet-} \rightarrow O^{\bullet-} + O_2$	2.6×10^3	2
52	$O_3^{\bullet-} + HO_2^- \rightarrow O_2^{\bullet-} + HO^- + O_2$	8.9×10^5	42
53	$O_3^{\bullet-} + H_2O_2 \rightarrow O_2^{\bullet-} + H_2O + O_2$	1.6×10^6	46
54	$HO_3^\bullet \rightarrow HO^\bullet + O_2$	1.1×10^5	58, 59
55	$HO_3^\bullet + HO_3^\bullet \rightarrow 2O_2 + H_2O_2$	5.0×10^9	57
56	$O_3 + HO^- \rightarrow O_2 + HO_2^-$	4.8×10^1	60
57	$O_3 + HO_2^- \rightarrow O_2 + HO^\bullet + O_2^-$	2.8×10^6	61
58	$O_3 + H_2O_2 \rightarrow O_2 + HO^\bullet + HO_2^\bullet$	3.7×10^{-2}	62
59	$HO_2^- + H_2O_2 \rightarrow H_2O + O_2 + HO^-$	4.5×10^{-4}	63

RSC Advances

ARTICLE

Table 2 Acido-basic equilibria, acidity constants and rate constants used in the simulation input file of the irradiation of aqueous solutions of sodium hydroxide, pH = 13.2, in presence of various concentrations of H_2O_2 added prior to the irradiations.

Number	Reaction	pKa	Ref.	k (M^{-1} s^{-1})	Ref.
60	$e_s^- + H_2O \rightarrow H^\bullet + HO^- + H_2O$	9.77	[3]	1.0×10^3	[64]
61	$H^\bullet + HO^- \rightarrow e_s^-$			2.5×10^7	[65]
62	$O^{\bullet-} + H_2O \rightarrow HO^\bullet + HO^-$	11.9	[3]	1.8×10^6	[2]
63	$HO^\bullet + HO^- \rightarrow O^{\bullet-} + H_2O$			1.3×10^{10}	[66]
64	$O_2^{\bullet-} + H_2O \rightarrow HO_2^\bullet + HO^-$	4.80	[67]	1.4×10^{-1}	[19]
65	$HO_2^\bullet + HO^- \rightarrow O_2^{\bullet-} + H_2O$			1.3×10^{10}	[49]
66	$O_3^{\bullet-} + H_2O \rightarrow HO_3^\bullet + HO^-$	6.45	[37]	2.5×10^1	
67	$HO_3^\bullet + HO^- \rightarrow O_3^{\bullet-} + H_2O$			5.1×10^{10}	
68	$H_2O + H_2O \rightarrow HO^- + H_3O^+$	13.99		6.5×10^{-7}	[19]
69	$HO^- + H_3O^+ \rightarrow H_2O + H_2O$			1.1×10^{11}	[49]
70	$O^{2-} + H_2O \rightarrow HO^- + HO^-$	36.00		1.0×10^{10}	
71	$HO^- + HO^- \rightarrow O^{2-} + H_2O$			1.0×10^{-10}	estimation
72	$HO_2^- + H_2O \rightarrow H_2O_2 + HO^-$	11.68	[68]	4.7×10^4	
73	$H_2O_2 + HO^- \rightarrow HO_2^- + H_2O$			5.4×10^8	[69]
74	$O2^{2-} + H_2O \rightarrow HO_2^- + HO^-$	16.50	[70]	1.1×10^6	[69]
75	$HO_2^- + HO^- \rightarrow O_2^{2-} + H_2O$			3.5×10^5	
76	$Na^+ + HO^- \rightarrow NaOH_0$	14.20	[68]	1.0×10^9	
77	$NaOH_0 \rightarrow Na^+ + HO^-$			2.9×10^9	

Table 3 Primary radiolytic yield values of radical and molecular species at pH = 13.2 as a function of the ionizing radiation source. Reference values of $G(HO^\bullet/O^{\bullet-})$ and $G(H_2O_2/HO_2^-)$ for our simulation model are written in red. The origin of these values is given in the discussion section with corresponding references.

Ionizing Radiation source	G (molecules/100eV)					
	e_s^-	$H^\bullet$	$HO^\bullet/O^{\bullet-}$	$HO_2^\bullet/O_2^{\bullet-}$	H_2O_2/HO_2^-	H_2
β	2.80	0.55	3.00	--	0.60	4.25×10^{-1}
C^{6+}	1.40	0.01	0.65	0.01	0.96	5.95×10^{-1}
	1.40	0.01	0.65	0.01	0.5	1.35×10^{-1}
	1.40	0.01	0.65	0.01	1.50	1.13
	1.40	0.01	0.65	0.01	2.00	1.63

In fact, our attempt in determining the value of $G(H_2O_2/HO_2^-)$ began first by the determination of $G(HO^\bullet/O^{\bullet-})$ in order to properly fit the initial absorption values recorded experimentally. For this purpose, we reasonably fixed its value at 0.65 molecules/100 eV which seemed to be in good agreement with experiment. This is explained through reaction 28 where $O^{\bullet-}$ formed through reaction 64 upon the passage of C^{6+} ion beams reacts with O_2 present in solution to form $O_3^{\bullet-}$. Reaction 28 is in equilibrium with reaction 51. Plus, the $G(HO^\bullet/O^{\bullet-})$ value of 0.65 molecules/100 eV is also in agreement with the value reported at 100 ns by Balcerzyk e*t al.* in 2014 when using O^{8+} of 1.2 GeV having the same order of magnitude for LET.[6]

The G value of $HO_2^\bullet/O_2^{\bullet-}$ is considered negligible. Yet, it is more befitting to fix it at 0.01 molecules/100 eV, a value reported when LET is equal to 33 eV/nm.[71] This latter value was also used for $H^\bullet$ since its yield is also considered to be negligible. Add to that, since the hydrated electron (e_{aq}^-) distribution is wider than that of other species, some electrons might escape the ion track. Therefore, its radiolytic yield value along with the one for hydronium ions is fixed at 1.4 molecules/100 eV. The radiolytic yield for molecular hydrogen has been obtained by taking into consideration the material balance of water decomposition and henceforth the fundamental relation between oxidizing and reducing species formed upon water decomposition as shown in Equation 1.

$$3 \cdot G(HO_2^\bullet) + 2 \cdot G(H_2O_2) + G(HO^\bullet) = 2 \cdot G(H_2) + G(e_{aq}^-) + G(H^\bullet) \quad (1)$$

We then found that the best fit is obtained when
$G(H_2O_2/HO_2^-) = 0.96$ molecule/100 eV
which is in agreement with literature.[71] The variation of H_2O_2 had to be handled carefully since a slight change in its value impacted the value of $G(H_2)$ by either obtaining negative or

Journal Name

ARTICLE

extremely high values which are immediately rejected since they represent forbidden conditions.

Conclusion

Water radiolysis mechanism in strongly alkaline solution remains bulk and incomplete. Many rate constant values of reactions involving ROS are in need of being revisited.

Almost stable in alkaline media, $O_3^{\bullet-}$ monitoring is shown to be possible without complications. Simulations of its formation and decay showed that in order to properly fit the kinetic, the rate constants of reaction between $O_3^{\bullet-}$ and HO_2^- need to be fixed at 1.1×10^6 rather than 8.9×10^5 M^{-1} s^{-1}. Furthermore, the rate constant of reaction between $O_3^{\bullet-}$ and $O_2^{\bullet-}$ need also to be re-evaluated at 1.5×10^7 rather than 10^4 M^{-1} s^{-1} in order to fully fit the recorded transient absorption.

Add to that, we evaluated $G(H_2O_2/HO_2^-)$ and $G(HO^\bullet/O^{\bullet-})$ for irradiations with high LET GeV-carbon ion beams. The values obtained were 0.96 and 0.65 molecules/100eV respectively. These values do not differ at all from what is already evaluated in the recent literature because of the fast equilibrium establishment within the non-homogeneous stage of the radiolysis scheme, and the fast scavenging of $O^{\bullet-}$ by O_2 in these present studies. These values are directly available for long time process in waste management.

Continuing the revisiting procedure for the other reactions in strongly alkaline solution (i.e. white lines in Table 1) supposes also to record the kinetics in other conditions of gas saturation, temperature, for instance, and/or change of detected species since $O_3^{\bullet-}$ and $O_2^{\bullet-}$ could be both achieved in an accessible wavelength domain. The help of Monte Carlo simulations should also allow the determination of primary radiolytic yields in these extreme conditions of pH as it was attempted recently with public or home-made programs including non-homogeneous water radiolysis mechanism.[12, 72, 73]

Acknowledgements

References

1. Y. Hatano, Y. Katsumura and A. Mozumder, *Charged Particle and Photon Interactions with Matter. Recent Advances, Applications, and Interfaces.*, CRC Press, Taylor and Francis Group, Boca Raton, 2011.
2. A. J. Elliot and D. M. Bartels, *The Reaction Set, Rate Constants and g-Values for the Simulation of the Radiolysis of Light Water over the Range 20° to 350°C Based on Information Available in 2008.*, Report AECL-153-127160-450-001, AECL, Mississauga, Ontario, Canada, 2009.
3. G. V. Buxton, C. L. Greenstock, W. P. Helman and A. B. Ross, *Journal of Physical and Chemical Reference Data*, 1988, **17**, 513-886.
4. C. Ferradini and J. P. Jay-Gerin, *Canadian Journal of Chemistry-Revue Canadienne De Chimie*, 1999, **77**, 1542-1575.
5. M. Lin, Y. Muroya, G. Baldacchino and Y. Katsumura, in *Recent Trends in Radiation Chemistry*, eds. B. S. M. Rao and J. F. Wishart, 2010.
6. A. Balcerzyk, I. Boughattas, S. Pin, E. Balanzat and G. Baldacchino, *Physical Chemistry Chemical Physics*, 2014, **16**, 23975-23984.
7. S. Yamashita, K. Iwamatsu, Y. Maehashi, M. Taguchi, K. Hata, Y. Muroya and Y. Katsumura, *Rsc Advances*, 2015, **5**, 25877-25886.
8. P. Bouniol, in *Radiation Chemistry: From Basics to Applications in Material and Life Sciences*, eds. M. Spotheim-Maurizot, M. Mostafavi, T. Douki and J. Belloni, EDP SCIENCES, 2008, ch. 8, pp. 117-129.
9. E. Hayon, *Transactions of the Faraday Society*, 1965, **61**, 734-743.
10. M. Haïssinsky, in *Actions chimiques et biologiques des radiations*, ed. M. Haïssinsky, Masson et Cie, Paris, 1967, pp. 131-179.
11. C. Ferradini and J. P. Jay-Gerin, *Research on Chemical Intermediates*, 2000, **26**, 549-565.
12. V. Cobut, C. Corbel and J. P. Patau, *Radiation Physics and Chemistry*, 2005, **72**, 207-215.
13. J. W. T. Spinks and R. J. Woods, *An introduction to radiation chemistry*, Wiley, New York, 3rd edn., 1990.
14. K. I. Priyadarsini, in *Charged Particle and Photon Interactions with Matter: Recent Advances, Applications, and Interfaces*, eds. Y. Hatano, Y. Katsumura and A. Mozumder, CRC Press, Boca Raton, 2010, ch. 22, pp. 595-622.
15. F. Haber and J. Weiss, *Proceedings of the Royal Society of London. Series A - Mathematical and Physical Sciences*, 1934, **147**, 332-351.
16. P. George, *Discussions of the Faraday Society*, 1947, **2**, 196-205.
17. B. Halliwell, *FEBS Letters*, 1976, **72**, 8-10.
18. G. J. McClune and J. A. Fee, *FEBS Letters*, 1976, **67**, 294-298.
19. P. Bouniol and E. Bjergbakke, *Journal of Nuclear Materials*, 2008, **372**, 1-15.
20. S. J. Blanksby, V. M. Bierbaum, G. B. Ellison and S. Kato, *Angewandte Chemie*, 2007, **119**, 5036-5038.
21. F. Si, X. Zhang and K. Yan, *Rsc Advances*, 2014, **4**, 5860-5866.
22. G. L. Hug, *Optical spectra of nonmetallic inorganic transient species in aqueous solution*, U.S. Dept. of Commerce, National Bureau of Standards, Washington, D.C., 1981.
23. B. H. J. Bielski and A. O. Allen, *Journal of Physical Chemistry*, 1977, **81**, 1048-1050.
24. J. Chlistunoff and J. P. Simonin, *Journal of Physical Chemistry A*, 2006, **110**, 13868-13876.
25. V. Wasselin-Trupin, G. Baldacchino, S. Bouffard, E. Balanzat, M. Gardes-Albert, Z. Abedinzadeh, D. Jore, S. Deycard and B. Hickel, *Journal of Physical Chemistry A*, 2000, **104**, 8709-8714.
26. G. Baldacchino, S. Bouffard, E. Balanzat, M. Gardès-Albert, Z. Abedinzadeh, D. Jore, S. Deycard and B. Hickel, *Nuclear Instruments and Methods in Physics Research Section B: Beam Interactions with Materials and Atoms*, 1998, **146**, 528-532.
27. G. Baldacchino, G. Vigneron, J. P. Renault, S. Pin, S. Rémita, Z. Abedinzadeh, S. Deycard, E. Balanzat, S. Bouffard, M. Gardès-Albert, B. Hickel and J. C. Mialocq, *Nuclear Instruments and Methods in Physics Research Section B: Beam Interactions with Materials and Atoms*, 2003, **209**, 219-223.
28. G. Baldacchino, G. Vigneron, J. P. Renault, S. Pin, Z. Abedinzadeh, S. Deycard, E. Balanzat, S. Bouffard, M. Gardès-

Albert, B. Hickel and J. C. Mialocq, *Chemical Physics Letters*, 2004, **385**, 66-71.

29. J.-C. Mialocq, B. Hickel, G. Baldacchino and M. Juillard, *J. Chim. Phys.*, 1999, **96**, 35-43.

30. B. H. Milosavljevic and J. A. LaVerne, *The Journal of Physical Chemistry A*, 2004, **109**, 165-168.

31. G. V. Buxton and C. R. Stuart, *Journal of the Chemical Society, Faraday Transactions*, 1995, **91**, 279-281.

32. J. F. Ziegler, M. D. Ziegler and J. P. Biersack, *Nuclear Instruments & Methods in Physics Research Section B-Beam Interactions with Materials and Atoms*, 2010, **268**, 1818-1823.

33. P. Kirkegaard, E. Bjergbakke and J. V. Olsen, *CHEMSIMUL: A chemical kinetics software package*, Report Risoe-R-1630, Risoe National Laboratory, 2008.

34. Farhataziz and M. A. J. Rodgers, *Radiation Chemistry - Principles and Applications*, VCH Publishers, New York, 1987.

35. W. L. Marshall and E. U. Franck, *Journal of Physical and Chemical Reference Data*, 1981, **10**, 295-304.

36. W. Wagner and A. Pruß, *Journal of Physical and Chemical Reference Data*, 2002, **31**, 387-535.

37. H. Tomiyasu, H. Fukutomi and G. Gordon, *Inorganic Chemistry*, 1985, **24**, 2962-2966.

38. K. Sehested, J. Holcman, E. Bjergbakke and E. J. Hart, *The Journal of Physical Chemistry*, 1982, **86**, 2066-2069.

39. E. Janata, M. Kelm and B. G. Ershov, *Radiation Physics and Chemistry*, 2002, **63**, 157-160.

40. G. Baldacchino, G. Vigneron, J. P. Renault, S. Le Caer, S. Pin, J. C. Mialocq, E. Balanzat and S. Bouffard, *Nuclear Instruments & Methods in Physics Research - Section B: Beam Interaction with Materials and Atoms*, 2006, 288-291.

41. V. Wasselin-Trupin, G. Baldacchino, S. Bouffard and B. Hickel, *Radiation Physics and Chemistry*, 2002, **65**, 53-61.

42. W. D. Felix, B. L. Gall and L. M. Dorfman, *The Journal of Physical Chemistry*, 1967, **71**, 384-392.

43. J. Rabani, in *Radiation Chemistry*, AMERICAN CHEMICAL SOCIETY, 1968, vol. 81, ch. 9, pp. 131-152.

44. M. S. Alam and E. Janata, *Chemical Physics Letters*, 2006, **417**, 363-366.

45. B. H. J. Bielski, *Photochem. Photobiol.*, 1978, **28**, 645-649.

46. G. Czapski, *The Journal of Physical Chemistry*, 1967, **71**, 1683-1688.

47. J. Weinstein and B. H. J. Bielski, *Journal of the American Chemical Society*, 1979, **101**, 58-62.

48. M. C. Sauer, W. G. Brown and E. J. Hart, *The Journal of Physical Chemistry*, 1984, **88**, 1398-1400.

49. A. J. Elliot, *Rate Constants and G-Values for the Simulation of the Radiolysis of Light Water over the Range 0-300 °C*, Report Report AECL-11073, Atomic Energy of Canada Limited, Chalk River, Ontario, Canada, 1994.

50. B. Pastina and J. A. LaVerne, *J. Phys. Chem. A*, 2001, **105**, 9316-9322.

51. K. Sehested, J. Holcman and E. J. Hart, *The Journal of Physical Chemistry*, 1983, **87**, 1951-1954.

52. E. Bjergbakke, D. Dragarne Z, K. Sehested and I. G. Dragarne, *Radiochimica Acta*, 1989, **48**, 65-72.

53. S. P. Mezyk and D. M. Bartels, *Journal of the Chemical Society, Faraday Transactions*, 1995, **91**, 3127-3132.

54. A. J. Elliot and G. V. Buxton, *Journal of the Chemical Society, Faraday Transactions*, 1992, **88**, 2465-2470.

55. E. Bjergbakke, K. Sehested, O. Lang Rasmussen and H. Christensen, *Input Files for Computer Simulation of Water Radiolysis*, Danmarks Tekniske Universitet, Risø Nationallaboratoriet for Bæredygtig Energi, 1984.

56. K. Sehested, J. Holcman, E. Bjergbakke and E. J. Hart, *The Journal of Physical Chemistry*, 1984, **88**, 269-273.

57. J. Staehelin, R. E. Buehler and J. Hoigne, *The Journal of Physical Chemistry*, 1984, **88**, 5999-6004.

58. R. Bühler, J. Staehelin and J. Hoigne, *The Journal of Physical Chemistry*, 1984, **88**, 2560-2564.

59. R. Bühler, J. Staehelin and J. Hoigne, *The Journal of Physical Chemistry*, 1984, **88**, 5450-5450.

60. L. Forni, D. Bahnemann and E. J. Hart, *The Journal of Physical Chemistry*, 1982, **86**, 255-259.

61. J. Staehelin and J. Hoigne, *Environmental Science & Technology*, 1982, **16**, 676-681.

62. K. Sehested, H. Corfitzen, J. Holcman and E. J. Hart, *The Journal of Physical Chemistry*, 1992, **96**, 1005-1009.

63. F. R. Duke and T. W. Haas, *The Journal of Physical Chemistry*, 1961, **65**, 304-306.

64. H. A. Schwarz, *The Journal of Physical Chemistry*, 1992, **96**, 8937-8941.

65. P. Han and D. M. Bartels, *The Journal of Physical Chemistry*, 1992, **96**, 4899-4906.

66. G. V. Buxton, *Transactions of the Faraday Society*, 1970, **66**, 1656-1660.

67. B. H. J. Bielski, D. E. Cabelli, R. L. Arudi and A. B. Ross, *Journal of Physical and Chemical Reference Data*, 1985, **14**, 1041-1100.

68. E. L. Shock, D. C. Sassani, M. Willis and D. A. Sverjensky, *Geochimica et Cosmochimica Acta*, 1997, **61**, 907-950.

69. T. Lundström, H. Christensen and K. Sehested, *Radiation Physics and Chemistry*, 2002, **64**, 29-33.

70. J. Jacq and O. Bloch, *Electrochimica Acta*, 1970, **15**, 1945-1966.

71. J. A. LaVerne, in *Charged Particle and Photon Interactions with Matter: Chemical, Physicochemical, and Biological Consequences with Applications*, eds. A. Mozumder and Y. Hatano, CRC Press, 2003, ch. 14, pp. 403-430.

72. M. Karamitros, S. Luan, M. A. Bernal, J. Allison, G. Baldacchino, M. Davidkova, Z. Francis, W. Friedland, V. Ivantchenko, A. Ivantchenko, A. Mantero, P. Nieminem, G. Santin, H. N. Tran, V. Stepan and S. Incerti, *Journal of Computational Physics*, 2014, **274**, 841-882.

73. L. M. Kohan, S. Sanguanmith, J. Meesungnoen, P. Causey, C. R. Stuart and J.-P. Jay-Gerin, *Rsc Advances*, 2013, **3**, 19282-19299.